energy&fuels

pubs.acs.org/EF
Article

Characterization of Energy-Relevant Liquid Products from Vacuum Pyrolysis of HDPE Microplastic

Hugo F. Brandolini, Marcelo L. Cocco, Edilton N. Silva, Jamilson Silva, Jr., Wanderson Romão, Lays Rafalscky, and Robson C. Sousa*

Cite This: https://doi.org/10.1021/acs.energyfuels.5c06298

ABSTRACT: In this study, the thermal degradation of high-density polyethylene (HDPE) microplastics was investigated to obtain and characterize the liquid fraction generated by vacuum pyrolysis, assessing its potential for energy valorization as an alternative fuel. The methodology included thermo-chemical characterization and mathematical modeling of HDPE based on thermogravimetric analyses conducted at heating rates of 5, 10, 15, 20, and 25 °C min^{-1}, differential scanning calorimetry (DSC), and vacuum pyrolysis performed under the following operational conditions: 550 °C, −100 mmHg, and a residence time of 90 min. The resulting oily liquid product was characterized by gas chromatography−mass spectrometry (GC-MS) and by high-resolution mass spectrometry (HRMS) using direct infusion with electrospray ionization and atmospheric pressure chemical ionization sources. The DTG and DSC results indicated that the onset of thermal degradation of the HDPE molecular chains occurred at approximately 500 °C. The comparison between experimental and predicted data demonstrated good agreement, validating the applicability of these methods for modeling the thermal degradation kinetics. The GC-MS analysis revealed that the liquid fraction is composed mainly of hydrocarbons, particularly alkanes (saturated chains) and alkenes (unsaturated chains). Furthermore, HRMS analysis confirmed, through Van Krevelen diagrams, that the liquid product is highly heterogeneous, exhibiting a predominance of linear and saturated alkanes similar to those found in light oils. Minor contributions from $O_x[H]$ and $N_xO_y[H]$ classes were also detected, likely associated with impurities and highly condensed aromatic species formed via aromatization and polycondensation reactions during pyrolysis.

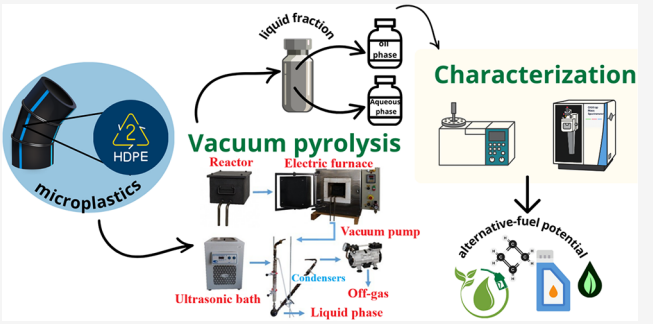

1. INTRODUCTION

Microplastics are characterized by their extremely small size (<5 mm), and they contaminate marine organisms such as fish and shellfish, since water can enter not only through the digestive system but also through the respiratory tract, accumulating in muscle fibers.[1] In addition, due to their variable porosity, microplastic particles are capable of adsorbing heavy metals, toxic molecules such as pesticides, and other highly harmful organic contaminants. This issue can directly affect populations that rely on fishing, since these toxic compounds propagate through the food chain via bioaccumulation.[2]

Recent studies have shown that environments with high concentrations of microplastics can interfere with the biological functioning of fish, amphibians, and even small mammals.[1,3−5] Microplastic particles have also been detected in humans—found in organs such as the heart, liver, kidneys, and brain, as well as in the placenta and breast milk.[6−8]—indicating that even newborns are not free from contamination, although the long-term health effects remain unknown.

In order to mitigate these impacts, increasing efforts have been directed toward reusing plastic materials so they can be reintegrated into different production cycles through reuse, recycling, depolymerization, or conversion into oils for fuel applications, among other applications.[9−11] High-density polyethylene (HDPE) is widely used in rigid packaging, such as medicine bottles and cleaning-product containers, and its secondary degradation reactions can generate liquid fractions (light and heavy oils) ranging from 40 to 60%.[11−13]

Several studies have investigated the thermal degradation of HDPE aiming at liquid fuel production under atmospheric pressure conditions. These works mainly focus on the influence of operational parameters such as temperature, heating rate, and residence time on product yields and chemical composition. However, detailed molecular-level characterization and systematic evaluation of the energy-related properties of liquid fractions

Received: December 1, 2025
Revised: January 27, 2026
Accepted: February 4, 2026

remain limited in these studies.[11−13,21,22] Most studies focus on alternative strategies such as catalytic pyrolysis, which employs catalysts to accelerate the thermal decomposition of the material.,[14−16] or copyrolysis, which combines HDPE with biomass to enhance the yield of condensable liquids and overall process efficiency.[17,18] However, systematic investigations specifically addressing HDPE under vacuum pyrolysis conditions, as well as comprehensive characterizations of the energy quality of the resulting liquid fraction —remain scarce. Vacuum pyrolysis of HDPE is still an underexplored field in the literature.

Recent research combining vacuum conditions with catalysts has yielded promising results, reinforcing the energy potential of the liquid phase produced from HDPE pyrolysis. Tekade et al.[19] demonstrated that the combination of vacuum and heterogeneous metal oxide catalysts can direct reaction selectivity, promoting the formation of specific carbon-chain structures while reducing undesirable compounds.

Although catalytic and pyrolysis routes have been extensively investigated, as pointed out in the study by Kalauni et al.,[20] the literature remains incipient regarding the systematic evaluation of HDPE under vacuum pyrolysis conditions. Despite the increasing interest in pyrolysis processes, limited attention has been given to the comprehensive characterization of the liquid fraction obtained under vacuum conditions. In particular, the careful assessment of its physical, chemical, and thermodynamic properties, as well as the detailed identification of its chemical composition, remains largely unexplored. To address this gap, the present study provides novel insights into the liquid phase derived from vacuum pyrolysis, contributing to a deeper understanding of its potential for energy valorization.

Studies that focus on the liquid fraction from HDPE pyrolysis predominantly report the use of GC-MS for chemical characterization.[21,22] Although GC-MS offers well-established advantages, it presents important limitations, such as low sensitivity for detecting species with carbon numbers above C_{45} and reduced ionization efficiency for compounds containing heteroatoms.[23] In this context, high-resolution mass spectrometry ($m/\Delta m_{50}\% \approx$ 480,000, with $\Delta m_{50}\%$ corresponding to full peak width at half-maximum at m/z 200) and mass accuracy below 1 ppm emerges as a robust alternative capable of substantially expanding molecular characterization ($C_cH_hN_nO_oS_s$). The application of this technique represents one of the key differentiating features of the present study.[24,25]

Therefore, this study, the thermal degradation of high-density polyethylene (HDPE) microplastics was investigated to obtain and characterize the liquid fraction generated by vacuum pyrolysis, assessing its potential for energy valorization as an alternative fuel. The methodology included the physical and thermo-chemical characterization of HDPE based on average particle size (d_p), true density (ρ_r), bulk density (ρ_b), bed porosity (ε), thermogravimetric analyses (TGA) at heating rates of 5, 10, 15, 20, and 25 °C min^{-1}, differential scanning calorimetry (DSC), and vacuum pyrolysis conducted at 550 °C and −100 mmHg. The liquid fraction obtained from pyrolysis was subsequently characterized by gas chromatography (GC-MS) coupled with high-resolution Orbitrap mass spectrometry (HRMS).

2. MATERIALS AND METHODS

This section describes the high-density polyethylene (HDPE) used in this study for physicochemical characterization, the experimental procedures employed, and the methods applied to estimate the parameters associated with its energy potential.

2.1. Preparation of HDPE Samples

High-density polyethylene (HDPE) was obtained from discarded packaging of food, pharmaceutical, and cleaning products. The containers were washed, manually cut, and milled in a knife mill (EcoEducacional) to reduce particle size. The resulting material—referred to as HDPE particulates—is shown in Figure 1.

Figure 1. High-density polyethylene (HDPE) particulates.

2.2. Thermal, Chemical, and Physical Characterization

2.2.1. Characterization of HDPE Particulates. HDPE particulates were characterized based on physical properties including particle size, true density, crystalline phase, and porosity. The true density (ρ_r) was determined by gas pycnometry using an Anton Paar Ultrapyc 3000 pycnometer and nitrogen 5.0 (N_2) as the working gas. The bulk density (ρ_b) was determined by compacting the particulate material in a 100 [mL] graduated cylinder.[26] After determining the mass of the solid and the total volume occupied by the particulates in the beaker, the bulk density was calculated according to eq 1 for $\forall_b$, considering the sum of the volume of the solid in the graduated cylinder and the volume of voids in the bed (bed porosity).

$$\rho_b = \frac{m_s}{\forall_b} \tag{1}$$

Bed porosity (ε) was indirectly determined using the ratio between bulk density (ρ_b) and true density (ρ_r), following eq 2.

$$\varepsilon = 1 - \frac{\rho_b}{\rho_r} \tag{2}$$

The crystalline phase of HDPE was identified by means of X-ray diffraction at room temperature, using a 2θ range of 1°−45°, a scan rate of 2° min^{-1}, and a step of 0.02°. This analysis yielded insights into the structural properties of the material.

Particle size was calculated from the Sauter mean diameter expression ($\bar{d}_p$) (eq 3), where x_i represents the mass fraction retained on each sieve, and d_i corresponds to the average sieve opening. A total sample mass of 87 g was used in the standardized sieves ranging from 4 to 32 mesh.

$$\bar{d}_p = \frac{1}{\int_0^1 \frac{dx}{d_\#}} \approx \frac{1}{\sum_{i=1}^{n} \frac{x_i}{d_i}} \tag{3}$$

Based on the particle size analysis, the cumulative weight fraction y_i was estimated and the models listed in Table 1 were applied accordingly.

Statistical analysis of the physical characterization results was performed in triplicate using Microsoft Excel to calculate standard deviation, standard error, 95% confidence intervals, and the coefficient of variation. Fitting of the granulometric models was performed using OriginPro 8.5, which yielded correlation coefficients (R^2), F-value, parameter estimates (n and m), their associated standard errors, and t tests.

https://doi.org/10.1021/acs.energyfuels.5c06298
Energy Fuels XXXX, XXX, XXX−XXX

Table 1. Mathematical Models for Estimating the Cumulative Particle-Size Frequency Distribution

model	equation	parameters	refs
RRB	$y_i = 1 - \exp\left[-\left(\frac{d_i}{D_{63.2}}\right)^n\right]$ (4)	n and $D_{63.2}$	27
GGS	$y_i = \left(\frac{d_i}{D_{100}}\right)^m$ (5)	m and D_{100}	27
Sigmoid	$y_i = \frac{1}{1 + \left(\frac{D_{50}}{d_i}\right)^n}$ (6)	n and D_{50}	28

2.3. Thermal Characterization: Thermogravimetric Analysis (TG), Differential Scanning Calorimetry (DSC), and Energetic Parameters (Ignition Temperature (T_i), Burnout Temperature (T_b), and Combustion Index (S))

Approximately 17 mg of HDPE particulates were analyzed using a LabSys EVO TGA/DSC system under a controlled N_2 atmosphere. The samples were heated at rates of 5, 10, 15, 20, and 25 °C min^{-1} up to a final temperature of 900 °C. Ignition (T_i) and burnout (T_b) temperatures were determined using the intersection-point method proposed by Lu and Chen[29] and Carvalho et al.[30] The combustion index (S) was calculated using eq 7, which incorporates T_i, T_B, and DTG parameters as defined by JIA.[31]

$$S = \frac{\mathrm{DTG_{max}} \times \mathrm{DTG_{med}}}{T_i^2 T_b} \tag{7}$$

where $\mathrm{DTG_{max}}$ is the peak value of the DTG curve and $\mathrm{DTG_{med}}$ is the average DTG value for each heating rate.

2.3.1. Mathematical Treatment—Isoconversional Methods. The rate of thermal degradation was expressed in terms of conversion (α) using eq 8.

$$\frac{d\alpha}{dt} = k(T) f(\alpha) \tag{8}$$

The Arrhenius eq (eq 9), together with the reaction mechanism $f(\alpha) = (1 - \alpha)^n$, defines the differential reaction model, in which n is the reaction order and α\alpha$\alpha$ is defined by eq 10.

$$k(T) = A \exp\left(\frac{-E_a}{RT}\right) \tag{9}$$

$$\alpha = \frac{m_0 - m}{m_0 - m_f} \tag{10}$$

The following variables were used: initial mass (m_0), final mass (m_f), instantaneous mass (m_t), pre-exponential factor (A), activation energy (E_a), temperature (T), and universal gas constant (R).

The isoconversional methods of Friedman, Kissinger–Akahira–Sunose (KAS), and Flynn–Wall–Ozawa (FWO) were applied according to eqs 11–13.

$$\ln\left(\frac{d\alpha}{dt}\right)_\alpha = \ln[Af(\alpha)]_\alpha - \frac{E_{a\alpha}}{RT_\alpha} \tag{11}$$

$$\ln\left(\frac{\beta}{T2}\right)_\alpha = \ln\left[\frac{AR}{E_a g(\alpha)}\right]_\alpha - \frac{E_{a\alpha}}{RT_\alpha} \tag{12}$$

$$\log(\beta)_\alpha = \log\left[\frac{AE_a}{Rg(\alpha)}\right]_\alpha - 2.3015 - 0.457\frac{E_{a\alpha}}{RT_\alpha} \tag{13}$$

The Friedman method was linearized so that, for each conversion degree, a data set is generated and treated as a straight line of the form $y = mx + b$, where $=\ln\left(\frac{d\alpha}{dt}\right)$, $x = \frac{1}{T}$, $b = \ln[Af(\alpha)]$ and slope $m = \frac{-E_a}{R}$.[32]

From the slope of the linear fit obtained at a given conversion level (α), the activation energy E_a was determined using the relation described in eq 14.[32−34]

$$E_a = -mR \tag{14}$$

where m is the slope of the fitted line and R is the universal gas constant (8.314 J mol^{-1} K^{-1}).

For the Friedman method (eq 11), the pre-exponential factor (A) was directly determined because the equation used to estimate the activation energy does not allow explicit separation of this parameter without prior knowledge of the conversion function $f(\alpha)$.[34] This occurs because the term $\ln[Af(\alpha)]$ appears as the intercept in the linearized equation, making it difficult to extract the exact value of A without additional assumptions regarding the underlying kinetic model.

To determine the kinetic parameters of thermal degradation (activation energy, pre-exponential factor, and reaction order), the isoconversional methods of Friedman, KAS, and FWO were implemented using the Python programming language. Because the pre-exponential factor cannot be analytically calculated using the FWO and KAS methods, the compensation-effect methodology, as employed by Sbirrazzuoli,[35] was applied. Accordingly, the value of A at each conversion level was calculated using eqs 15 and 16

$$A_\alpha = \frac{E_{a\alpha} \exp(C_\alpha) g(\alpha)}{R} \tag{15}$$

$$A_\alpha = \frac{10^{C_\alpha + 2,315} g(\alpha) R}{E_{a\alpha}} \tag{16}$$

where C_α represents the intercept for each conversion level in the regression analyses of the methods, following the relation ($\ln(A_\alpha) = aE_a + b$), yielding the expression $A = \exp(aE_a + b)$.

The activation energy and the pre-exponential factor were obtained by implementing the isoconversional methods of Friedman, KAS, and FWO for first-order reaction kinetics, also adopted by Khedri,[36] using the Python programming language. The activation energy was determined from the slope of the linear fits according to the methodology of each model at each conversion level.

2.4. Statistical Evaluation of Isoconversional Models

The quality of the model was evaluated using the coefficient of determination (R^2), the sum of squared residuals (SSR), and the total sum of squares (SST). These statistical parameters were computed using the scikit-learn library in Python, as expressed in eqs 17–19.

$$\mathrm{SST} = \sum_i (x_{\mathrm{exp},i} - \underline{x}_{\mathrm{exp},i})^2 \tag{17}$$

$$R^2 = 1 - \frac{\sum_{i=1}^n (x_{\mathrm{exp},.i} - x_{\mathrm{pred},i})^2}{\sum_{i=1}^n (x_{\mathrm{exp},i} - \underline{x}_{\mathrm{exp},i})^2} \tag{18}$$

$$\mathrm{SSR} = \sum_i (x_{\mathrm{exp},.i} - x_{\mathrm{pred},i})^2 \tag{19}$$

where x_{pred}, x_{exp} and $\overline{x}_{\mathrm{exp}}$ denote the predicted, experimental, and mean experimental values, respectively.

2.5. Thermodynamic Parameters

Thermodynamic parameters — enthalpy (ΔH), Gibbs free energy (ΔG), and entropy (ΔS) — were calculated following Ahmad et al.,[37] Alves et al.,[38] and Kaur et al.,[39] using eqs 20–22

$$\Delta H = E_\alpha - RT_\alpha \tag{20}$$

$$\Delta G = E_\alpha + RT_m \ln = (K_B T_m / hA) \tag{21}$$

$$\Delta S = (\Delta H - \Delta G)/T_m \tag{22}$$

where T_α is the temperature at a given conversion (K), T_m the DTG peak temperature (K), A the pre-exponential factor (s^{-1}), R the gas constant ($R = 0.008314$ kJ mol^{-1} K^{-1}), K_B the Boltzmann constant (K_B

https://doi.org/10.1021/acs.energyfuels.5c06298
Energy Fuels XXXX, XXX, XXX−XXX

= 1.381×10^{-26} kJ K^{-1}), and h the Planck constant ($h = 6.626 \times 10^{-37}$ kJ s).

2.6. Vacuum Pyrolysis Apparatus and Operating Conditions

The experimental unit (Figure 2) consisted of a stainless-steel reactor treatment box (120 × 150 × 180 mm^3) for HDPE particulates, a

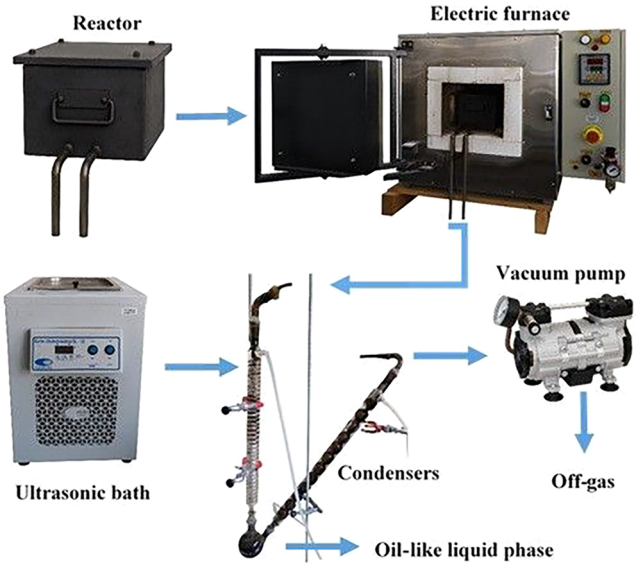

Figure 2. Experimental unit for vacuum-pyrolysis comprising the reactor treatment, electric furnace, condensation system, and vacuum pump.

Fortelab muffle furnace (Model FCN-1200; 10 L chamber; maximum temperature 1200 °C; power 14 kW), a condensation system comprising two condensers connected in series and cooled by an ultrathermostatic bath (Solab SL-152), and a LabECO 740 vacuum pump capable of reaching −760 mmHg.

A particulate HDPE sample (40 g) was placed inside the treatment reactor, manually sealed, inserted into the furnace, and connected to the condensation system. The cooling bath was set to 10 °C to ensure circulation of chilled water through the condensers.

Vacuum pyrolysis was performed at a heating rate of 10 °C min^{-1} until 550 °C, which was held for 90 min. A digital PID controller (Flyever) regulated furnace temperature, and vacuum (−100 mmHg) was supplied by the pump. A type-K thermocouple monitored internal reactor temperature, and two PT-100 thermocouples monitored furnace and reactor temperatures. Data acquisition was performed using FlexLab software.

At the end of pyrolysis, the cooling bath temperature was increased to 28 °C to recover the wax accumulated in the round-bottom flask connected to the condenser. The liquid fraction was centrifuged to separate aqueous and oily phases.

2.7. Characterization of the Liquid Fraction from Vacuum Pyrolysis

2.7.1. Gas Chromatography−Mass Spectrometry (GC-MS). Gas chromatography−mass spectrometry (GC−MS) analysis was performed using an Agilent 6890 GC system coupled to a 5973 MSD. Compound separation was achieved on an Rtx-5MS column (30 m × 0.25 mm × 0.25 μm film thickness). The temperature program was initiated at 40 °C, held for 2 min, and then ramped to 240 °C at 3 °C min^{-1}, where it was held for 10 min. The injector temperature was set to 220 °C. Homogeneous solutions were prepared by diluting the liquid phase in dichloromethane following the methodology of Natesakhawat et al.[22] The solutions were injected individually into the nonpolar column using helium as the carrier gas at a constant flow of 1.78 mL min^{-1}. Ionization was performed by electron impact at 70 eV. During the analysis, the ion source and interface were held at controlled temperatures of 200 and 240 °C, respectively. Pyrolysis-oil components were identified using the instrument software and the NIST mass spectral libraries.

2.7.2. High-Resolution Orbitrap Mass Spectrometry (HRMS). To complement the GC−MS characterization, the oil sample was analyzed by high-resolution mass spectrometry (HRMS) using an Orbitrap Exploris 480 mass spectrometer (Thermo Fisher Scientific, Bremen, Germany). Three ionization modes were employed: electrospray ionization (ESI) in positive (ESI(+)) and negative (ESI(−)) modes, and atmospheric-pressure chemical ionization in positive mode (APCI(+)). In all cases, data were acquired over a mass range of 200−1000 Da.

ESI(±) analyses, the oil sample was prepared at 1 mg mL^{-1} using a toluene/methanol solvent mixture (1:1, v/v). To promote ionization in positive mode, 1% formic acid (v/v) was added, whereas 1% NH_4OH was used for negative mode. Direct-injection flow was set to 10 μL min^{-1}. Capillary voltages were 3000 V (ESI(+)) and 2500 V (ESI(−)). The ion transfer tube temperature was set to 300 °C. Source parameters were: sheath gas 10 au, auxiliary gas 10 au, and sweep gas 0 au For APCI(+) analyses, the oil sample was prepared at 1.5 mg mL^{-1} in a disulfide:isooctane mixture (1:3, v/v), adapted from Tose et al.[40] Direct-injection flow was 10 μL min^{-1}. Corona discharge was set to 5 au The source and ion transfer tube temperatures were both maintained at 300 °C. Gas parameters were: sheath gas 35 au, auxiliary gas 10 au, and sweep gas 0 au.

Spectral processing was performed using a custom algorithm in Composer software (Sierra Analytics, Pasadena, CA).[41] Elemental compositions were assigned, enabling construction of class distributions, DBE (double bond equivalent) vs carbon number (NC) plots, DBE-intensity distributions, and van Krevelen diagrams. DBE corresponds to the number of rings and/or double-bond equivalents in each molecular structure. Equation 23 provides DBE values, where C, H, and N denote the number of carbon, hydrogen, and nitrogen atoms, respectively.

$$\mathrm{DBE} = C - \frac{H}{2} + \frac{N}{2} + 1 \tag{23}$$

Based on the DBE versus carbon number (NC) plots and the mass accuracy (<1 ppm), it was possible to propose tentative molecular structures. These assignments were made using the PubChem database (National Library of Medicine, NLM).

3. RESULTS AND DISCUSSION

3.1. Structural Characterization of the HDPE Particulate: Sauter Mean Diameter ($\bar{d}_p$), Density (ρ_r), X-ray Diffraction Analysis (XRD), and Porosity (ε)

The physical characterization results for the HDPE particulates used in this study are presented in Table 2. The average particle size was approximately 2.40 mm, while the true density, bulk density, and porosity values were 969.56 kg m^{-3}, 331.96 kg m^{-3}, and 0.6576, respectively.

Statistical analysis confirmed significance at the 95% confidence level, as standard deviations remained lower than the measured averages. In addition, t-values greater than 1 and coefficients of variation below 10% ensured good reproducibility.

Table 2. Particulates Characterization Data Obtained in Triplicate with a 95% Confidence Level for All Variables

property	mean value	95% confidence interval	coefficient of variation (%)
$\bar{d}$[mm]	2.394 ± 0.023	0.207	0.96
ρ_b [kg m^{-3}]	331.96 ± 13.50	33.54	4.07
ρ_r [kg m^{-3}]	969.56 ± 1.53	1.89	0.16
ε [-]	0.6576	-	-

https://doi.org/10.1021/acs.energyfuels.5c06298
Energy Fuels XXXX, XXX, XXX−XXX

Figure 3 shows the cumulative particle-size distribution of the HDPE particulate. Approximately 35% of the sample exhibited a

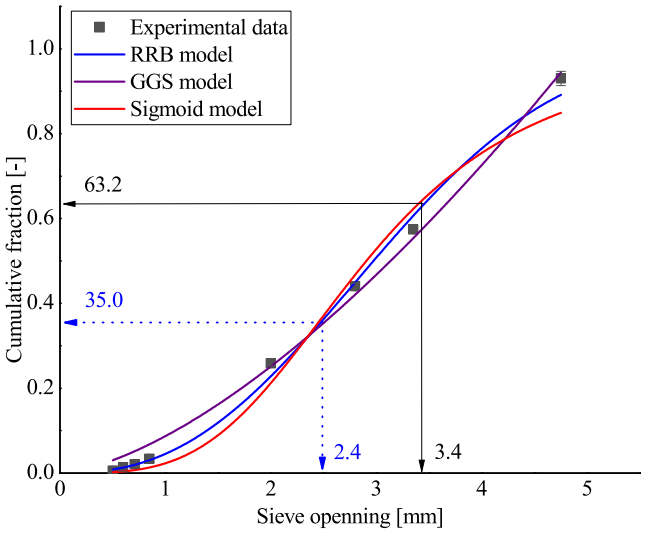

Figure 3. Cumulative fractions of the HDPE particulate.

diameter smaller than 2.40 mm, whereas the RRB model predicted that 63.2% of the particles had diameters smaller than 3.44 mm.

The RRB model provided the best fit to the experimental data, as indicated by its high *F*-value (1260.33) and coefficient of determination (R^2 = 0.9950) and high *t* test values for $D_{63.2}$ (57.42), demonstrating that these values lie far lie far beyond the associated estimation errors (Table S1).

The X-ray diffraction (XRD) data of the HDPE particulates (Figure S5) identified three main diffraction peaks at 21.5°, 24°, and 36.1°, consistent with the characteristic crystalline structure of HDPE.[42] Additional minor peaks were also observed, likely associated with impurities or additives (e.g., antioxidants, colorants), which are commonly present in commercial polymeric materials.

The physical characterization of the HDPE material unequivocally confirms that the samples used in this study fall within the dimensional criteria established for microplastics. The Sauter mean diameter of 2.40 mm, the RRB-predicted cumulative distributions showing that more than half of the particles remain below 3.44 mm, and the narrow confidence intervals associated with these measurements collectively demonstrate that the particulate material is consistently smaller than the 5 mm threshold defined for microplastic classification. Complementary properties—including a high bed porosity (ε = 0.6576), a true density of 969.56 kg m^{-3}, and a bulk density of 331.96 kg m^{-3}. Together, these results validate that the HDPE particulate employed in the pyrolysis experiments is structurally and dimensionally consistent with microplastics.

3.2. Thermochemical Characterization by Thermogravimetry (TG/DTG) and Differential Scanning Calorimetry (DSC)

Figure 4 displays the TG and DTG curves for HDPE particulates at heating rates of 5−25 °C min^{-1}.

The thermogravimetric curves (Figure 4a) and the derivative curve (Figure 4b) exhibit a single and abrupt decomposition event at approximately 500 °C, indicating high thermal stability, as also reported by Das and Tiwari[43] and Natesakhawat et al.[22] This single-stage decomposition suggests that the HDPE particulates undergo a relatively homogeneous thermal degradation process, without significant intermediate steps, which is consistent with the behavior expected for polymers with a predominantly linear molecular structure and lacking complex branching.

Complete thermal degradation of HDPE occurred between 500 and 600 °C, a temperature range in which the residual mass of the polymer becomes constant, indicating the completion of the process. This information is essential for defining the operating temperature in the pyrolysis process, ensuring that all polymer chains are effectively decomposed and converted into volatile, liquid, or gaseous products without leaving significant residues.

Figure 5 shows the heat flow profiles obtained by differential scanning calorimetry (DSC).

Two distinct temperature ranges can be distinguished, highlighted by vertical lines, within which the heat flow magnitude increases, indicating significant thermal events during heating. The initial and final temperatures defining each range correspond to the points at which the heat flow

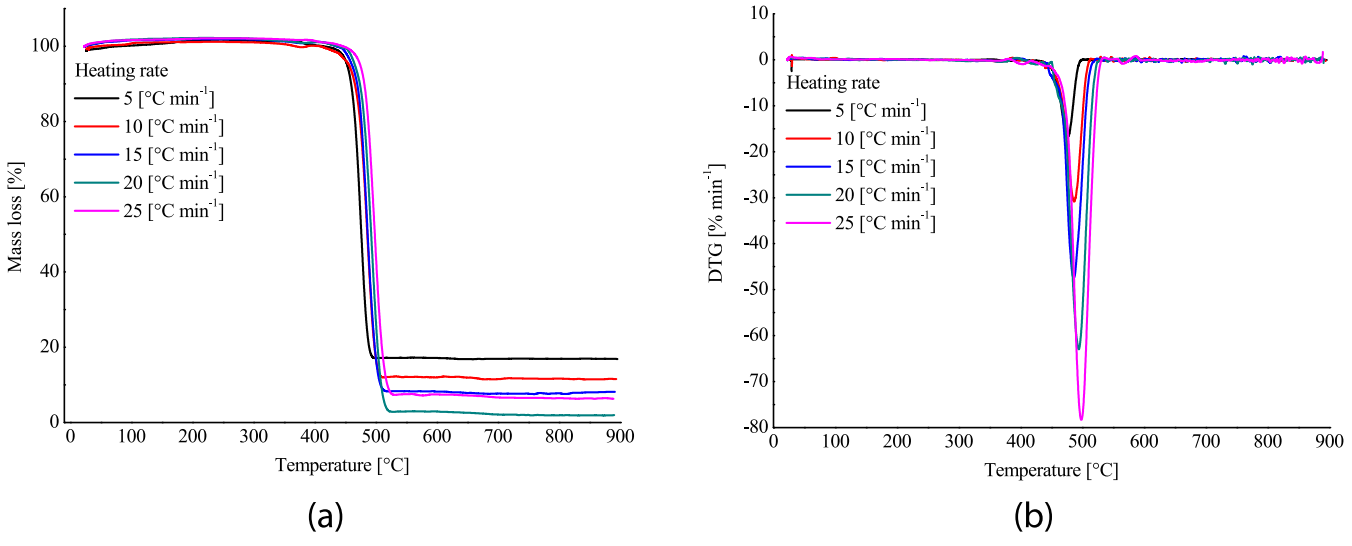

Figure 4. Thermochemical data for HDPE particles: (a) thermogravimetric (TG) curves and (b) derivative thermogravimetry (DTG).

https://doi.org/10.1021/acs.energyfuels.5c06298
Energy Fuels XXXX, XXX, XXX−XXX

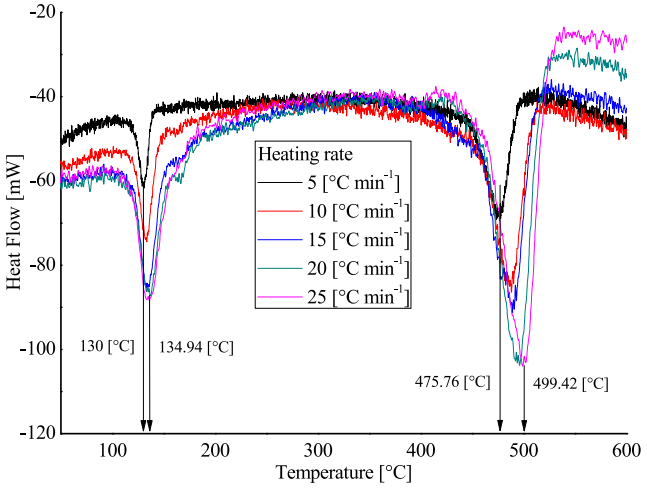

Figure 5. Differential scanning calorimetry (DSC) data for the HDPE particulates.

reaches local minima at heating rates of 5 and 25 °C min^{-1}. These minima correspond to critical thermal transitions associated with structural changes in the material.

Studies conducted by Furukawa et al.[44] report that the temperature range between 130 and 134.94 °C is indicative of polymer melting, characterized by the transition from the crystalline to the amorphous phase, where polymer chains gain mobility and the material loses rigidity. This temperature interval is associated with the energy required to disrupt the intermolecular interactions that stabilize the crystalline structure of the HDPE particulates. The temperature range between 475.76 and 499.42 °C represents the onset of thermal degradation of the HDPE macromolecules, marking the point at which carbon chains begin to break randomly, releasing volatile compounds and initiating the material's decomposition. The combined analysis of the DSC and TG/DTG data corroborated the selection of 550 °C as the operating temperature for the vacuum pyrolysis experiments.

3.3. Ignition Temperature (T_i), Burnout Temperature (T_b), and Combustion Index (S)

The results showed a slight tendency for the ignition (T_i) and burnout (T_b) temperatures to shift toward higher values with increasing heating rate (Figure S1). The T_i and T_b values used to calculate the combustion index (S), according to eq 7, are presented in Table 3.

The combustion index (S) for HDPE particulates remained nearly constant across all heating rates, behavior not commonly observed for other materials such as poultry manure, as reported by Carvalho et al.[30] The S value indicates good reactivity; however, the high ignition temperature of HDPE shows that a greater thermal energy input is required to initiate ignition.

Table 3. Data Used in Equation 7 to Calculate the Combustion Index (S)

rate (°C min^{-1})	$DTG_{máx}$ (%/min)	$DTG_{méd}$ (%/min)	T_i (°C)	T_b (°C)	S ($\times 10^{-7}$)
5	−3.494	−0.105	734.55	759.25	8.95
10	−3.148	−0.111	742.65	771.85	8.21
15	−3.263	−0.113	743.95	772.55	8.62
20	−3.176	−0.121	749.35	780.75	8.76
25	−3.247	−0.115	755.55	784.55	8.34

3.4. Thermochemical Parameters and Simulation of Isoconversional Models

The linear regressions of the isoconversional models applied in this study, conducted at heating rates of 10, 15, and 20 °C·min^{-1} (Friedman, KAS, and FWO), showed results consistent with those reported in the literature, with R^2 values approximately 0.99 across the conversion range, indicating excellent linearity (Figure S2). The mean activation energy (E_a) and pre-exponential factor (A) values are reported in Table 4.

Table 4. Activation Energy (E_a) and Pre-Exponential Factor (A) for the Thermal Degradation of HDPE

Método	E_a (kJ mol^{-1})	A ($1\ s^{-1}$)	R^2
Friedman	339.29 ± 38.36	3.51×10^{21}	0.99
KAS	340.30 ± 43.02	1.39×10^{21}	0.99
FWO	350.65 ± 27.77	1.17×10^{22}	0.99

As shown in Table 4, the activation energy values are similar within the standard deviation, and the pre-exponential factors are the order of 10^{21}−10^{22} s^{-1}. Natesakhawat et al.[22] reported E_a values of approximately 270 kJ mol^{-1} and A values on the order of 10^{19} s^{-1}. Similarly Sinfrônio et al.[45] reported activation energy values ranging from 306 to 476 kJ mol^{-1}, and pre-exponential factors on the order of 10^{14} to 10^{20} s^{-1}.

The simulation of the experimental and predicted thermogravimetric curves at 5, 10, 15, 20, and 25 °C min^{-1} showed good agreement (Figure S3), as further supported by the R^2, SST, and SSR metrics calculated from the comparison between model predictions and experimental TG data values (Table S2). These results confirm that the isoconversional models applied are suitable for describing the thermal degradation kinetics of HDPE under the conditions studied.

3.5. Thermodynamic Parameters of HDPE Thermal Decomposition: Activation Enthalpy (ΔH), Activation Entropy (ΔS), and Activation Gibbs Free Energy (ΔG)

The thermodynamic parameters associated with HDPE thermal degradation are presented in Figure 6a−c for activation enthalpy (ΔH), activation entropy (ΔS), and Gibbs free energy (ΔG) as functions of the conversion fraction (α). These parameters offer fundamental insights into the energetic requirements and molecular rearrangements involved in the decomposition process and complement the kinetic analysis discussed earlier.

The trend observed for ΔS (Figure 6b) follows a trend similar to that of ΔH. At low conversion levels, ΔS exhibits high positive values, indicating a market increase in system disorder associated with the formation of radical species and random chain cleavage. As degradation progresses, ΔS progressively decreases, suggesting the formation of more structurally organized products or fragments. This reduction in entropy indicates that although the system initially exhibits a substantial increase in disorder, the resulting decomposition products tend to exhibit reduced configurational freedom, consistent with observations reported in polymer degradation studies by Chee et al.[46]

Gibbs free energy (ΔG) remained positive across the entire conversion range (Figure 6c), indicating that HDPE degradation is a nonspontaneous process under the studied conditions and requires continuous thermal energy input. At the early stages of degradation, ΔG values exceeded 300 kJ mol^{-1}, but gradually decreased to the 250−300 kJ mol^{-1} range at higher conversion levels. This downward trend indicates a progressive

https://doi.org/10.1021/acs.energyfuels.5c06298
Energy Fuels XXXX, XXX, XXX−XXX

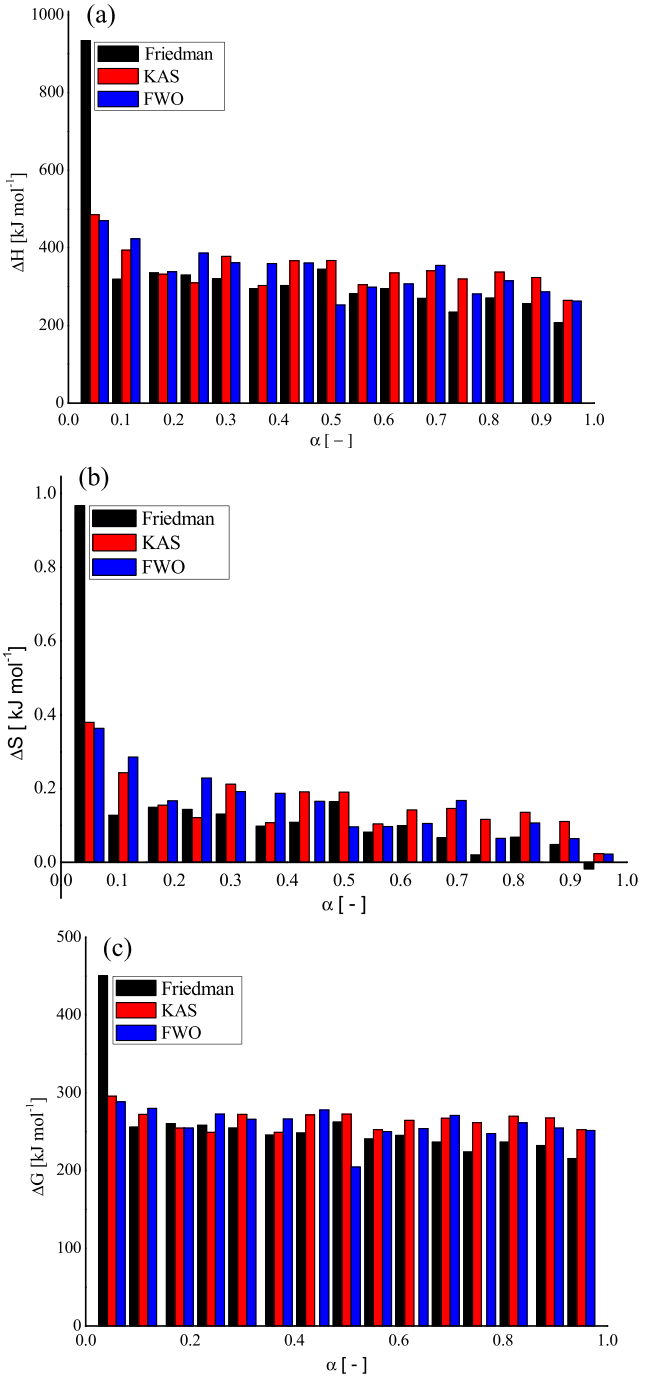

Figure 6. (a) shows that at the early stages of conversion (α = 0.05), ΔH exhibited slightly higher values, reflecting the additional energy required to initiate bond scission in the highly stable HDPE macromolecular structure. Once these initial bonds were broken, ΔH decreased and stabilized at approximately 300 kJ mol^{-1} across the remaining conversion range. This indicates that once thermal degradation has been initiated, the continuation of pyrolysis proceeds more easily, requiring less energy.

reduction in the thermodynamic barrier as the reaction advances, an effect often associated with the accumulation of reactive intermediates and increased disorder, which facilitates subsequent chain scission. Similar trends were reported by Meena and Bhoi[47] for the pyrolysis of thermoplastic materials.

The differences among the results obtained using the Friedman, KAS, and FWO methods can be attributed to the mathematical formulation of each model. The Friedman method, which is a differential, is inherently more sensitive to experimental noise, whereas the KAS and FWO integral methods exhibit smoother and more stable responses across the conversion range. These methodological distinctions explain the minor variations observed among the thermodynamic curves. Nonetheless, all models consistently indicate that HDPE pyrolysis is an endothermic process that requires continuous energy input and becomes progressively more thermodynamically favorable as degradation progresses.

3.6. Vacuum Pyrolysis

Vacuum pyrolysis of HDPE particulates was conducted using a heating rate of 10 °C min^{-1} until reaching 550 °C, which was then maintained for 90 min. Figure 7 shows the temperature profiles inside the treatment box and in the furnace during the process. The black line represents the external furnace temperature, while the red line depicts the internal temperature of the HDPE bed.

A pronounced temperature lag was observed between the two temperature measurements, indicating that the HDPE inside the sealed treatment box required significantly more time to reach the set point temperature. This slow heat transfer highlights the insulating effect of the metallic enclosure and the importance of a sufficiently long residence time to ensure uniform heating and complete degradation of the polymer. Notably, the internal temperature reached the target of 550 °C only after approximately 40 min of processing.

At the end of the pyrolysis experiment, the condensed liquid fraction and the past wax residue that accumulated in the condensation system were collected in a flat-bottom flask. Both products exhibited a dark yellow–brown coloration (Figure 8), which is characteristic of complex hydrocarbon mixtures containing hydrocarbon chains of varying lengths and degrees of unsaturation. The strong, pungent odor of the oil further suggests the presence of volatile and semivolatile organic compounds formed via random scission of polymer chains.

These observations agree with previous reports by Kumbar et al.[48] and Panda and Mahapatra,[13] who describe pyrolysis liquids as hydrocarbons-rich mixtures with properties similar to those of petroleum-derived fuels. The high flammability of the resulting liquids reinforces their potential for energy valorization, particularly in applications that require readily combustible feedstocks.

3.6.1. Gas Chromatography–Mass Spectrometry (GC–MS) of the Liquid Fraction. GC–MS analysis produced the chromatograms (Figure S3), allowing the identification of the molecular constituents of the liquid fraction. The chemical composition was composed exclusively of hydrocarbons, as expected for HDPE, which contains only carbon and hydrogen in its structure. The identified hydrocarbons included predominantly of alkanes (saturated hydrocarbons) and alkenes (unsaturated hydrocarbons containing carbon–carbon double bonds), with carbon numbers ranging from C_7 to C_{29}.

A considerable number of compounds exhibited terminal unsaturations, a common feature of thermal degradation processes in which random chain scission produces fragments bearing terminal double bonds. Additionally, cyclic hydrocarbons—such as 1-methylcyclohexene and cyclohexadecane were detected—indicating the occurrence of secondary reactions during pyrolysis, including cyclization and intramolecular rearrangements. The presence of branched alkenes, such as 2,4-dimethyl-1-heptene, further supports the influence

https://doi.org/10.1021/acs.energyfuels.5c06298
Energy Fuels XXXX, XXX, XXX–XXX

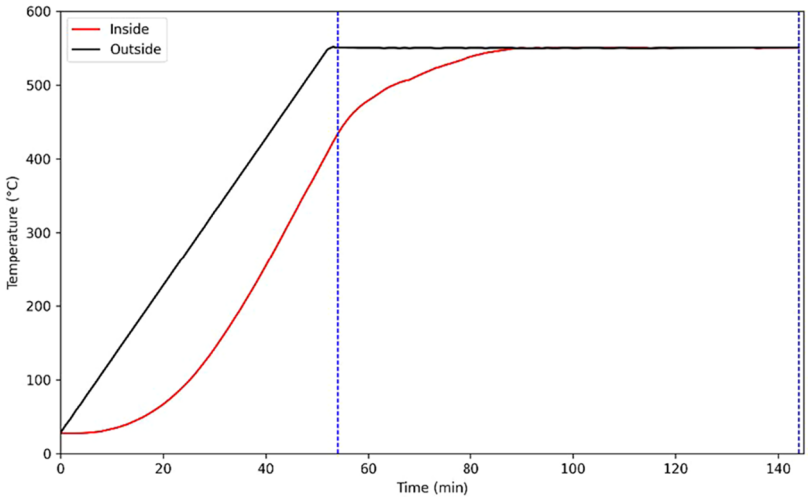

Figure 7. Temperature data inside the treatment box as a function of time (solid red line) and furnace temperature (solid black line).

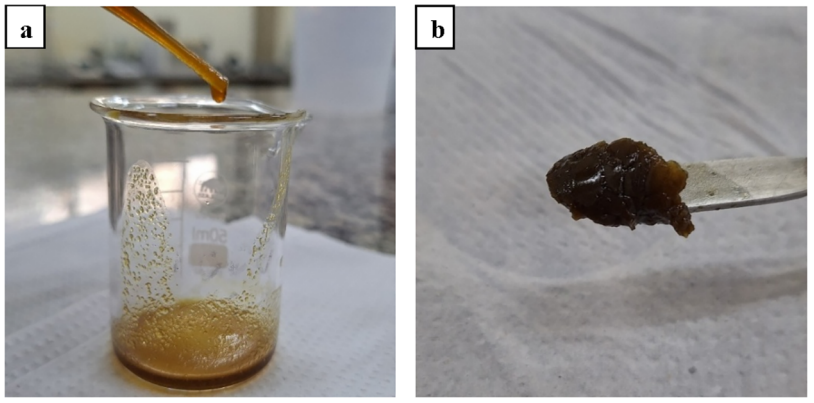

Figure 8. Products obtaneid from HDPE vacuum pyrolysis: (a) condensed liquid fraction and (b) past wax residue.

Table 5. Identified Compounds in the GC−MS Analysis of the Liquid Fraction

compounds	chemical fórmula	chemical class	compounds	chemical fórmula	chemical class
toluene	C_7H_8	aromatic	tridecane	$C_{13}H_{28}$	alkane
1-methylcyclohexene	C_7H_{12}	cycloalkene	1.13-tetradecadiene	$C_{14}H_{26}$	diene
ethylbenzene	C_8H_{10}	aromatic	tetradecane	$C_{14}H_{30}$	alkane
O-xylene	C_8H_{10}	aromatic	1.15-hexadecadiene	$C_{16}H_{30}$	diene
1-methylcycloheptene	C_8H_{14}	cycloalkene	1-hexadecene	$C_{16}H_{32}$	alkene
1-octene	C_8H_{16}	alkene	hexadecane	$C_{16}H_{34}$	alkane
octane	C_8H_{18}	alkane	1-heptadecene	$C_{17}H_{34}$	alkene
1.8-nonadiene	C_9H_{16}	aiene	heptadecane	$C_{17}H_{36}$	alkane
1-nonene	C_9H_{18}	alkene	1-octadecene	$C_{18}H_{36}$	alkene
2.4-dimethyl-1-heptene	C_9H_{18}	alkene	octadecane	$C_{18}H_{38}$	alkane
nonane	C_9H_{20}	alkane	1-nonadecene	$C_{19}H_{38}$	alkene
1.9-decadiene	$C_{10}H_{18}$	diene	nonadecane	$C_{19}H_{40}$	alkane
1-decene	$C_{10}H_{20}$	alkene	1.19-eicosadiene	$C_{20}H_{38}$	diene
decane	$C_{10}H_{22}$	alkane	eicosane	$C_{20}H_{42}$	alkane
3-undecyne	$C_{11}H_{20}$	alkyne	heneicosane	$C_{21}H_{44}$	alkane
1-undecene	$C_{11}H_{22}$	alkene	1.21-docosadiene	$C_{22}H_{42}$	diene
undecane	$C_{11}H_{24}$	alkane	1-docosene	$C_{22}H_{44}$	alkene
1.11-dodecadiene	$C_{12}H_{22}$	diene	*cis*-9-tricosene	$C_{23}H_{46}$	alkene
1-dodecene	$C_{12}H_{24}$	alkene	1-tricosene	$C_{23}H_{46}$	alkene
dodecane	$C_{12}H_{26}$	alkane	tricosane	$C_{23}H_{48}$	alkane
1-tridecene	$C_{13}H_{26}$	alkene	nonacosane	$C_{29}H_{60}$	alkane

of secondary transformations that typically accompany polymer pyrolysis processes.

Table 5 lists the compounds identified, along with their chemical formulas, and molar masses. Among these the

https://doi.org/10.1021/acs.energyfuels.5c06298
Energy Fuels XXXX, XXX, XXX−XXX

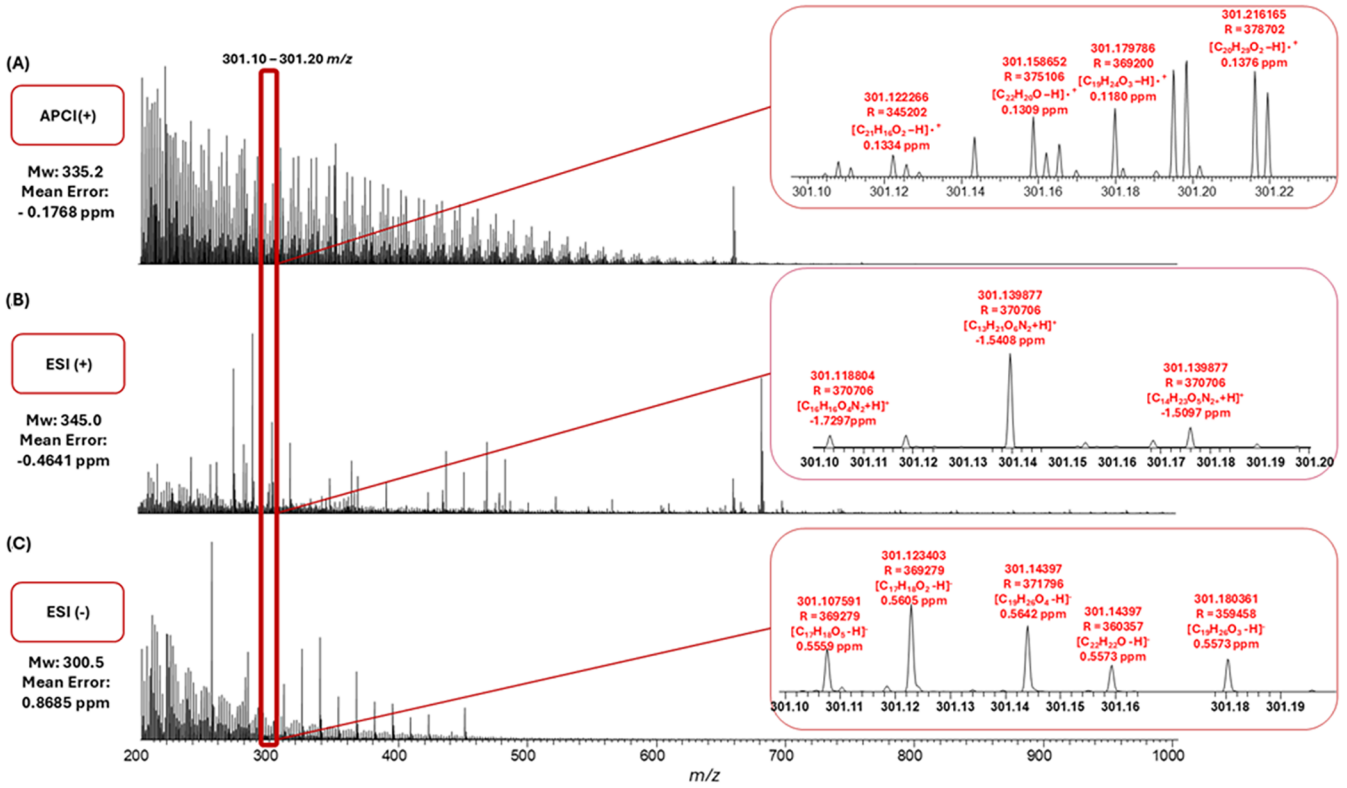

Figure 9. Mass spectra acquired on the Orbitrap MS 480 using (A) APCI(+) ionization; (B) ESI(+) ionization; and (C) ESI(−) ionization.

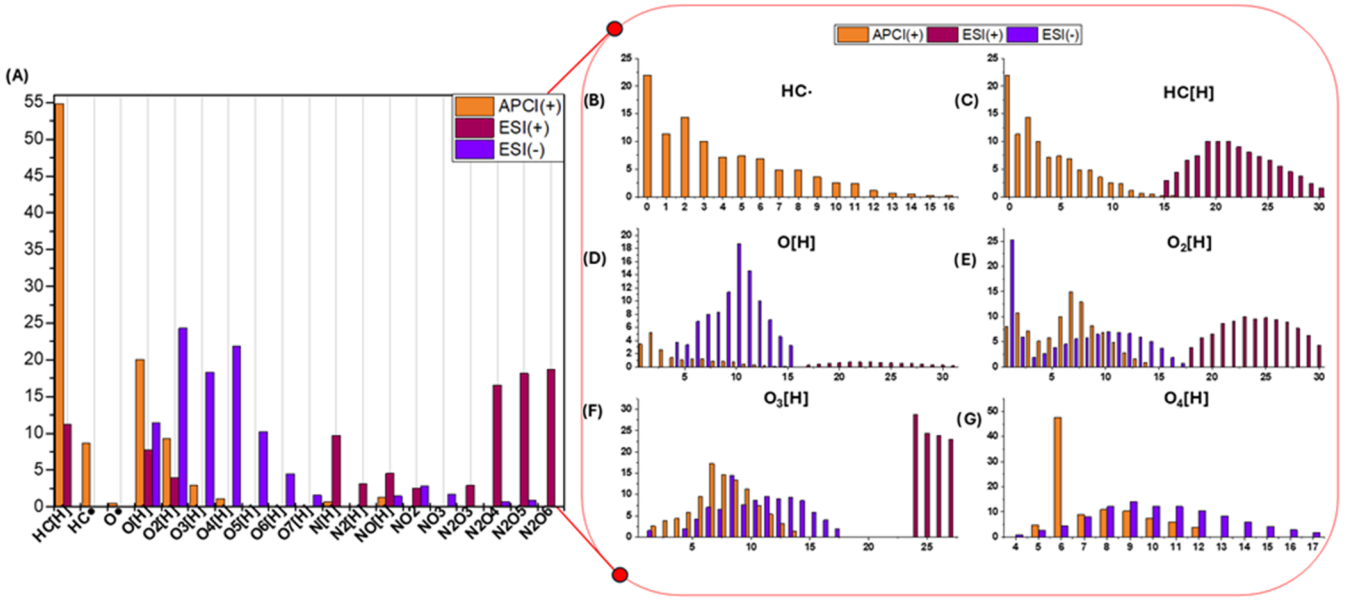

Figure 10. Class distribution and DBE-versus-intensity plots for the APCI(+), ESI(+), and ESI(−) ionization sources for the following classes: (B) HC•, (C) HC[H], (D) O[H], (E) O_2[H], (F) O_3[H], and (G) O_4[H].

constituents, common industrial and petrochemical molecules such as toluene, xylene, and octane were detected, reflecting the complex hydrocarbon profile of the condensable vapor-phase products.

In addition to these species, numerous alkenes and alkadienes with varying carbon-chain lengths were identified. Many compounds exhibited terminal double bonds, consistent with patterns previously reported by Al-Salem,[11] Natesakhawat et al.,[22] and Panda and Mahapatra.[13] Overall, the GC−MS results indicate that the liquid fraction produced from HDPE vacuum pyrolysis consists of a diverse mixture of hydrocarbons spanning linear, branched, and cyclic structures, further reaffirming their similarity to petrochemical-derived fuels.

It is important to note that the alcohols detected in the HPED-derived (Figure 10) pyrolysis liquid are most likely associated with impurities or secondary oxygenated species formed during processing thermal. Under the GC−MS analysis conditions employed in this study, particularly the injector

https://doi.org/10.1021/acs.energyfuels.5c06298
Energy Fuels XXXX, XXX, XXX−XXX

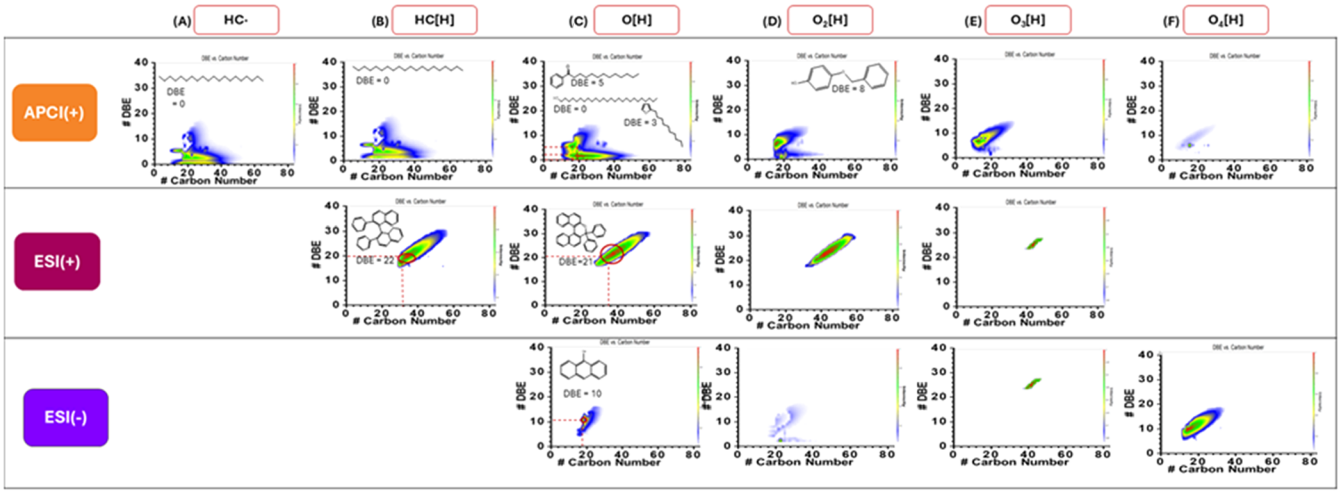

Figure 11. DBE versus carbon number plots for the APCI(+), ESI(+), and ESI(−) ionization sources for the classes (A) HC•; (B) HC[H]; (C) O[H]: (D) O2[H]; (E) O3[H] e (F) O4[H].

temperature of 220 °C, these alcohols may undergo partial thermal dehydration, leading to the *in situ* formation of the corresponding terminal olefins. As consequence, olefinic compounds detected in the chromatograms and mass spectra may not exclusively originate from the pyrolysis process itself, but may also result from transformations occurring during the injection step.

It should be noted that, under EI ionization at 70 eV, the mass spectra of terminal olefins may closely resemble those of their corresponding alcohols, especially for long-chain species. Although alcohols were detected only in trace amounts, this possible overlap was taken into account during peak assignment. Retention-time behavior and high-resolution MS data were used to improve discrimination; however, a minor degree of uncertainty between these two compounds cannot be entirely excluded.

3.6.2. High-Resolution Orbitrap Mass Spectrometry (HRMS) of the Liquid Fraction. The APCI(+) and ESI(±) Orbitrap MS spectra for the liquid phase (Figure 9A−C, respectively) were consistent with expectations for this type of organic matrix. Owing to the predominant hydrocarbons (HCs), —particularly the HC[H] and HC classes— a broader distribution of hydrocarbon was observed mainly under APCI(+), m/z 200−700 range, which enabled the identification of 1506 compounds. In contrast, under ESI(±) ionization, the number of detected signals was significantly lower, m/z 200−550 range, because this technique preferentially the ionization of polar species, which are present at very abundant in HDPE pyrolysis byproducts—namely nitrogen-containing classes (N_x, where x = 1 and 2) and mixed classes (N_xO_y, where x = 1−2 and y = 2−6) in ESI(+), and oxygenated classes (O_x, where x = 2−7) in ESI(−), as shown in Figure 10 Consequently, 1451 compounds were identified in ESI(+), with 71% formula assignment, a value considerably lower than that obtained with APCI(+), likely due to the lower signal abundance. In ESI(−), 1198 compounds were identified, with 82% assignment. In summary, magnification of the spectra in Figure 9 in the m/z 301.10−301.22 region shows that APCI(+) detected, in some cases, more than twice as many signals as the ESI(+) source (19 vs 7).

The class distribution diagram obtained from Orbitrap MS data processing (Figure 10A) shows the higher abundance of the HC[H] class under APCI(+) ionization. Although ESI(+) is not the most suitable technique for ionizing hydrocarbons, the high concentration of these species in the sample still enabled the detection of the HC[H] class with a measurable relative abundance (12%).

The DBE versus intensity plots (Figure 10B−G) demonstrate the effectiveness of this analytical approach for characterizing HDPE pyrolysis residues. In the HC and HC[H] classes (Figure 10B−C), the oil sample was primarily composed of linear and saturated structures (DBE ≈ 0), which are typical of alkanes commonly found in crude oil. This composition suggests potential applications as a fuel or petrochemical feedstock.[49,50] However, more complex and unsaturated molecules were also identified within these classes, with DBE values ranging from 1−15 in APCI(+) and >15 in ESI(+), indicating the presence of aromatic or condensed species.

In APCI(+), minor molecular classes were also detected, including O_x[H], where x = 1−4, and N_xO_y[H], where x = 1 and y = 0−1. In contrast, the ESI(−) source predominantly favored the detection of highly oxygenated compound classes, O_x[H], where x = 1−7, followed by mixed classes N_xO_y[H], where x = 1−2 and y = 1−5. Overall, it is evident that the ESI(±) ionization modes are more effective at detecting highly polar and aromatic species than APCI(+). Although pure HDPE is not expected to contain oxygen in its structure, a recent review by Snow et al.[51] highlights that residual heteroatoms may remain in the final oil. The authors also discuss challenges associated with removing nitrogen-, oxygen-, and chlorine-containing species from pyrolysis liquids. Belbessai et al.[52] note that raw pyrolysis products often carry impurities originating from the feedstock, additives, contaminants, and the reaction atmosphere, which supports the observation of O_x[H], N_x[H], and N_xO_y[H] classes. The presence of residual heteroatoms observed in the Orbitrap MS analysis was also detected in the XRD results (Figure S4), demonstrating coherence between the analytical techniques. Therefore, Orbitrap MS has proven to be more effective than GC−MS in detecting both nonpolar and polar chemical species, owing to its higher sensitivity, broader mass range (m/z 100−3000), and superior resolution, which together enable the identification of minor constituents in the liquid fraction.

https://doi.org/10.1021/acs.energyfuels.5c06298
Energy Fuels XXXX, XXX, XXX−XXX

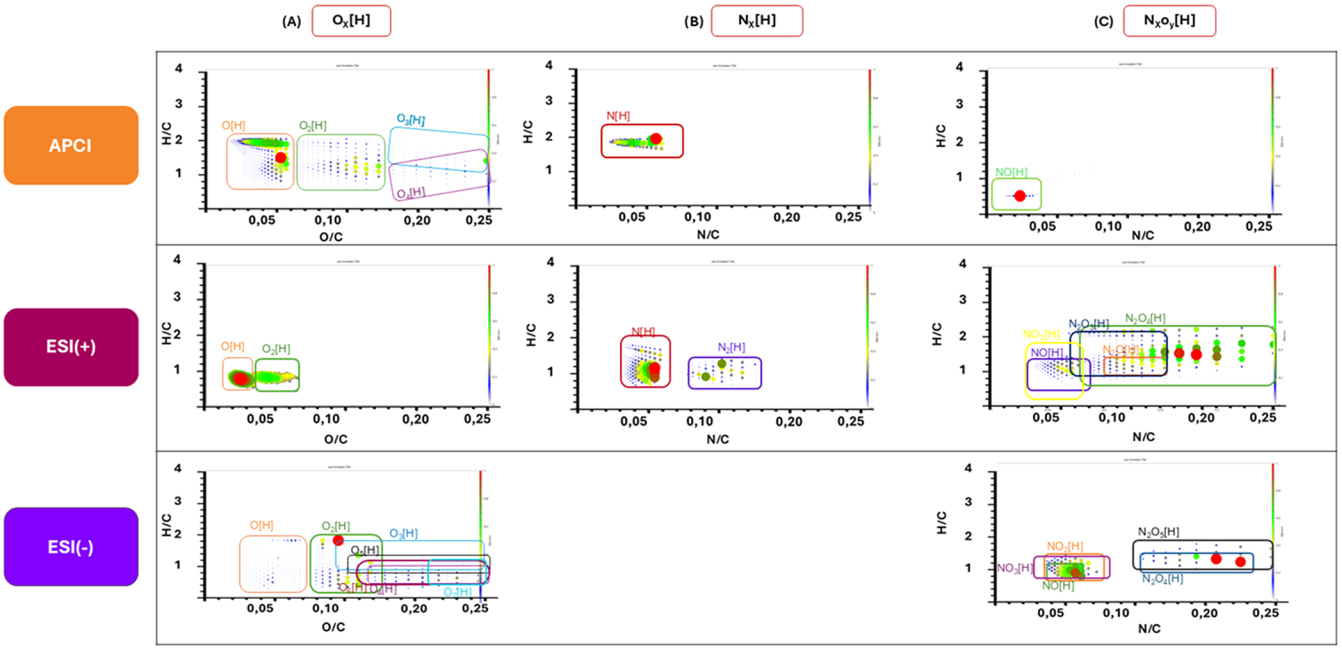

Figure 12. Van Krevelen diagrams for the APCI(+), ESI(+), and ESI(−) sources for the classes: (A) O_x[H], (B)N_x[H] e (C)N_xO_y[H].

The DBE versus carbon number (NC) plots for the HC•, HC[H], O[H], O_2[H], O_3[H], and O_4[H] classes (Figure 11) provide a two-dimensional representation of compound abundance. In these contour plots, color intensity reflects detection abundance: red regions indicate the highest-abundance zones, whereas light blue regions represent the least abundant. For APCI(+) data, the most abundant classes—HC•, HC[H], and O[H]—exhibited similar distribution patterns (Figure 11), with NC values ranging from C_{10} to C_{48} and DBE values from 0 to 18. The highest concentrations were centered around C_{20} and DBE = 0, which is characteristic of long-chain saturated hydrocarbons typical of paraffinic matrices. In contrast, the ESI(±) sources preferentially ionized highly aromatic and condensed. For ESI(+), NC values ranged from C_{26} to C_{56} with DBE values from 16 to 32 for the HC[H], O[H], and O_2[H] classes. For ESI(−), compounds ranged from C_{13} to C_{26} with DBE values from 4 to 18 for the O[H] and O_2[H] classes.[50]

An important aspect that cannot be disregarded is the formation artifacts generated by the ionization sources, at least for part of the identified classes.[53] During ESI and APCI ionization, partial *in-source* oxidation may occur due to radicals formed within the source or through reactions with residual oxygen present in the solvent or in the ionization region. The formation of clusters of the type $[M_1 + M_2 + H]^+$ may also generate ions that mimic molecular formulas containing additional heteroatoms.[53,54] In the study conducted by Pedersen and Conti,[55] different types of pure high-density plastics were used as feedstock in a hydrothermal process aimed at producing what the authors referred to as "synthetic petroleum." Although this hydrothermal system differs from pyrolysis, the authors demonstrated that the processing generated not only hydrocarbons but also monomeric chemical compounds such as terephthalic acid and bisphenol A.[55]

Under an inert atmosphere, such as during vacuum-assisted pyrolysis, the detection of heteroatoms containing species is rarely reported; yet such species may still be present in virgin plastics, as noted by Snow et al.[51] In the study by Kumar and Singh,[56] the authors reported only the presence of alkanes and alkenes in HDPE pyrolysis products. This is because the analytical method used—GC−MS—primarily detects hydrocarbons, thus inherently limiting the scope of the results.

The analysis of the Van Krevelen diagrams (Figure 12) clearly illustrates the structural heterogeneity of the pyrolysis oil. The highest compounds density is concentrated at H/C ≈ 2 and O/C values close to zero in APCI(+), which is consistent with the predominance of linear and saturated alkanes similar to those found in light crude oils. In contrast, minor populations at intermediate O/C ratios (up to 0.1) correspond to the O_x[H] and N_xO_y[H] classes detected by Orbitrap MS. These species are likely associated with impurities or secondary *in-source* oxidation products. Furthermore, compounds located around H/C ≈ 1 (in ESI(±)) indicate the presence of highly condensed aromatic species formed through aromatization and polycondensation reactions during pyrolysis, as described by Kumar and Singh[56] and Natesakhawat et al.[22]

4. CONCLUSION

In this study, the thermal degradation of high-density polyethylene (HDPE) was evaluated through thermochemical characterization and kinetic modeling. In addition, vacuum pyrolysis enable the production of a liquid fraction whose chemical composition and molecular characteristics indicate strong potential for energy valorization as an alternative fuel.

The HDPE particulate used in the pyrolysis experiments exhibited physical characteristics consistent with microplastics, presenting an average particle size with d_p < 4.0 mm, as confirmed by the Sauter mean diameter and the RRB model. This classification was further supported by the bulk porosity value of 0.6576 and the true and bulk densities of 969.56 and 331.96 kg m^{-3}, respectively.

Thermal degradation proceeded through a single stage mechanism, with mass loss occurring between 500 and 600 °C, as observed in the TG and DTG curves. The DSC heat-flow curves exhibited distinct minima at heating rates of 5 and 25 °C min^{-1}, indicating structural changes in the microplastic. In

https://doi.org/10.1021/acs.energyfuels.5c06298
Energy Fuels XXXX, XXX, XXX−XXX

addition, the temperature interval from 475.76 to 499.42 °C corresponds to the onset of thermal degradation of the molecular chains that constitute HDPE, which, together with the TG/DTG data, supported the selection of 550 °C as the operating temperature for the vacuum pyrolysis process.

The ignition and burnout temperatures increased from 734.55 to 755.55 K and from 759.25 to 784.55 K, respectively, with increasing heating rate from 5 to 25 °C min^{-1}. The combustion index (S) showed only a variation minimal variation across this range from 8.21 to 8.95×10^{-7}. The kinetic parameters obtained from the isoconversional Friedman, KAS, and FWO models yielded activation energy of 339.29 ± 38.36, 340.30 ± 43.02, and 350.65 ± 27.77 kJ mol^{-1}, respectively. The corresponding pre-exponential factors were 3.51×10^{21}, 1.39×10^{21}, and 1.17×10^{22}. The comparison between predicted and experimental results demonstrated good agreement, thus validating the applicability of the isoconversional methods for modeling the thermal degradation kinetics of HDPE.

The thermodynamic parameters ΔH and ΔG as a function of conversion (α) indicated that, after the onset of thermal degradation, the polymer chains process requires progressively less energy. The decrease in ΔS with increasing α reinforces that system disorder is highest at the beginning of the degradation process and stabilizes as smaller fragments are formed.

Vacuum pyrolysis of high-density polyethylene (HDPE) yielded both wax and an oily liquid fraction, whose composition consisted predominantly of hydrocarbons. GC−MS analysis of the liquid phase identified carbon-chain lengths ranging from C_7 to C_{29}, mainly alkanes (saturated chains) and alkenes (chains containing carbon−carbon double bonds). High-resolution Orbitrap results demonstrated that HDPE pyrolysis generates an oil with a predominantly paraffinic composition (>50%), composed of saturated hydrocarbons similar to those found in crude oil, accompanied by minor oxygenated and condensed aromatic fractions (<30%). Detailed analysis of the class distribution diagrams, DBE versus NC plots, and Van Krevelen diagrams showed that the resulting sample exhibits potential for applications as an alternative fuel due to its compositional similarity to synthetic crude oils. However, the data also revealed the need for additional purification and refining strategies owing to the significant presence of heteroatoms in the sample.

From an environmental perspective, HDPE pyrolysis proved to be a promising alternative for reducing the impact caused by the improper disposal of plastics. By converting plastic waste into useful products such as oils and waxes, this process contributes to decreasing dependence on fossil resources and minimizing the accumulation of waste in the environment. However, it is important to emphasize that the efficiency of the process and the quality of the resulting products depend on several factors, including the purity of the feedstock, the operational conditions, and the presence of catalysts, which can influence the selectivity of the reactions.

Although vacuum pyrolysis has proven effective in generating a hydrocarbon-rich liquid fraction from HDPE microplastics, its industrial implementation faces significant challenges. Large-scale operation must be conducted under stable low-pressure conditions, which requires robust sealing systems, high-efficiency vacuum pumps, and continuous pressure monitoring. Heat transfer limitations under vacuum may also restrict processing capacity, demanding optimized reactor geometries or auxiliary heating strategies. Additionally, the continuous feeding and discharging of HDPE under reduced pressure remain critical engineering hurdles, as does the integration of efficient condensation and separation units capable of handling complex vapor streams while preventing the release of gases into the working environment. Addressing these considerations is essential to enable the scale-up of vacuum pyrolysis from laboratory conditions to a feasible and reliable industrial technology.

■ ASSOCIATED CONTENT

Supporting Information

The Supporting Information is available free of charge at https://pubs.acs.org/doi/10.1021/acs.energyfuels.5c06298.

Statistical results for the mathematical models used to predict the cumulative particle-size distribution; ignition and burnout temperatures; predicted and experimental data obtained from the isoconversional models; statistical analyses for the Friedman, KAS, and FWO methods; the chromatogram of the liquid fraction; and the X-ray diffraction (XRD) of the HDPE particulate (PDF)

■ AUTHOR INFORMATION

Corresponding Author

Robson C. Sousa − *Laboratory of Transport Phenomena and Unit Operations (LaFTOP), Department of Chemical Engineering, Federal University of Espírito Santo, Alto Universitário, Alegre 29500-000 ES, Brazil;* orcid.org/0000-0002-2353-9098; Phone: +552835528603; Email: robson.sousa@ufes.br

Authors

Hugo F. Brandolini − *Laboratory of Transport Phenomena and Unit Operations (LaFTOP), Department of Chemical Engineering, Federal University of Espírito Santo, Alto Universitário, Alegre 29500-000 ES, Brazil;* orcid.org/0009-0008-6052-3678

Marcelo L. Cocco − *Laboratory of Transport Phenomena and Unit Operations (LaFTOP), Department of Chemical Engineering, Federal University of Espírito Santo, Alto Universitário, Alegre 29500-000 ES, Brazil*

Edilton N. Silva − *Laboratory of Transport Phenomena and Unit Operations (LaFTOP), Department of Chemical Engineering, Federal University of Espírito Santo, Alto Universitário, Alegre 29500-000 ES, Brazil*

Jamilson Silva, Jr. − *Laboratory of Transport Phenomena and Unit Operations (LaFTOP), Department of Chemical Engineering, Federal University of Espírito Santo, Alto Universitário, Alegre 29500-000 ES, Brazil*

Wanderson Romão − *Federal Institute of Education, Science and Technology of Espírito Santo, 29106-010 Vila Velha, Brazil;* orcid.org/0000-0002-2254-6683

Lays Rafalscky − *Federal University of Espírito Santo, 29075-910 Vitória, Espírito Santo, Brazil*

Complete contact information is available at: https://pubs.acs.org/10.1021/acs.energyfuels.5c06298

Author Contributions

E.N.S.: Data Curation, writing—original draft and Validation. M.L.C.: Mathematical modeling, data curation. J.S.J.: Data curation of thermogravimetric. H.F.B.: Writing review and editing and formal analysis, and characterization analysis chemical CG-MS. W.R.: Characterization analysis chemical HRMS Orbitrap, data curation, formal analysis, and writing

https://doi.org/10.1021/acs.energyfuels.5c06298
Energy Fuels XXXX, XXX, XXX−XXX

review and editing. L.R.: Analysis and data curation HRMS Orbitrap, and writing review and Editing. R.C.S.: Conceptualization, methodology and resources, investigation, formal analysis, visualization, writing—original draft, project administration, and funding Acquisition.

Funding

R.C.S. reports financial support was provided by Foundation for Research Support of Espírito Santo - Edital FAPES 28/2022 - Universal T.O 958/2023 Processo 2023-D407H. E.N.S. reports financial support was provided by Coordination for the improvement of Higher Education Personnel - Edital N 16/2022 - PDPG (grant 16/2022). The Article Processing Charge for the publication of this research was funded by the Coordenacao de Aperfeicoamento de Pessoal de Nivel Superior (CAPES), Brazil (ROR identifier: 00x0ma614).

Notes

The authors declare no competing financial interest.

■ ACKNOWLEDGMENTS

We acknowledge the use of ChatGPT (OpenAI) to support English language refinement, solely for grammar improvement, text organization, and structural editing of the manuscript. The authors would also like to thank the Laboratory of Transport Phenomena and Unit Operations (LaFTOP) and the Laboratory of Chemical Analysis and Materials Characterization (LaCMAT) of the Chemical Engineering Department at the Federal University of Espírito Santo (UFES). We further acknowledge the Multiuser Center for Technological Development and Innovation of Vila Velha (CMVV−Ifes) for their technical support in high-resolution mass spectrometry (HRMS) analyses, as well as Analytical Center I of the Graduate Program in Agrochemistry (UFES) for providing access to gas chromatography−mass spectrometry (GC−MS) facilities.

■ REFERENCES

(1) Akhbarizadeh, R.; Moore, F.; Keshavarzi, B. Investigating microplastics bioaccumulation and biomagnification in seafood from the Persian Gulf: a threat to human health? *Food Addit. Contam.,:Part A* **2019**, *36* (11), 1696−1708.

(2) Macleod, M.; Arp, H. P. H.; Tekman, M. B.; et al. The global threat from plastic pollution. *Science* **2021**, *373* (6550), 61−65.

(3) Gaspar, L.; Bartman, S.; Coppotelli, G.; et al. Acute Exposure to Microplastics Induced Changes in Behavior and Inflammation in Young and Old Mice. *Int. J. Mol. Sci.* **2023**, *24* (15), No. 12308.

(4) Ruthsatz, K.; Schwarz, A.; Gomez-Mestre, I.; et al. Life in plastic, it's not fantastic: Sublethal effects of polyethylene microplastics ingestion throughout amphibian metamorphosis. *Sci. Total Environ.* **2023**, *885*, No. 163779.

(5) Santos, D.; Luzio, A.; Félix, L.; et al. Microplastics and copper induce apoptosis, alter neurocircuits, and cause behavioral changes in zebrafish (Danio rerio) brain. *Ecotoxicol. Environ. Saf.* **2022**, *242*, No. 113926.

(6) Fournier, S. B.; D'Errico, J. N.; Adler, D. S.; et al. Nanopolystyrene translocation and fetal deposition after acute lung exposure during late-stage pregnancy. *Part. Fibre Toxicol.* **2020**, *17* (1), No. 55, DOI: 10.1186/s12989-020-00385-9.

(7) Kwon, W.; Kim, D.; Kim, H. Y.; et al. Microglial phagocytosis of polystyrene microplastics results in immune alteration and apoptosis in vitro and in vivo. *Sci. Total Environ.* **2022**, *807*, No. 150817.

(8) Ragusa, A.; Notarstefano, V.; Svelato, A.; et al. Raman Microspectroscopy Detection and Characterisation of Microplastics in Human Breastmilk. *Polymers* **2022**, *14* (13), No. 2700.

(9) Kabeyi, M. J. B.; Olanrewaju, O. A. Review and Design Overview of Plastic Waste-to-Pyrolysis Oil Conversion with Implications on the Energy Transition. *J. Energy* **2023**, *2023*, No. 1821129.

(10) Vijayakumar, A.; Sebastian, J. Pyrolysis process to produce fuel from different types of plastic - A review. *IOP Conf. Ser.:Mater. Sci. Eng.* **2018**, *396*, No. 012062, DOI: 10.1088/1757-899x/396/1/012062.

(11) Al-salem, S. M. In *Use of Polyethylene as a Feedstock for Value Added Product Recovery: Wax Recovery from Pyrolysis*, WIT Transactions on Engineering Sciences; WITPress, 2021; pp 93−99.

(12) Sambandam, P.; Punitha, N.; Vijetha, K.; et al. Effect of Graphite Nanoadditives on the Behavior of a Diesel Engine Fueled with Pyrolysis Fuel Recovered from Used Plastics. *ACS Omega* **2024**, *9* (38), 39584−39595.

(13) Panda, A. K.; Mahapatra, P. M. Pyrolytic Conversion of Waste High-Density Polyethylene to Wax: Temperature Optimization and Characterization of Wax. *Fine Chem. Eng.* **2024**, 221−229.

(14) Sharma, A.; Murugan, S. Potential for using a tyre pyrolysis oil-biodiesel blend in a diesel engine at different compression ratios. *Energy Convers. Manage.* **2015**, *93*, 289−297.

(15) Raveh-amit, H.; Lemont, F.; Bar-Nes, G.; et al. Catalytic pyrolysis of high-density polyethylene: Decomposition Efficiency and Kinetics. *Catalysts* **2022**, *12*, No. 140.

(16) Qie, Z.; Xiang, H.; Xiang, H.; et al. Catalytic pyrolysis of high-density polyethylene over hierarchical ZSM-5 zeolites produced by microwave-assisted chelation-alkaline treatment. *Fuel* **2024**, *368*, No. 131532.

(17) Rahman, M. H.; Bhoi, P. R.; Saha, A.; et al. Thermo-catalytic co-pyrolysis of biomass and high-density polyethylene (HDPE) towards improved pyrolysis liquid. *Energy* **2021**, *225*, No. 120231.

(18) Zulkafli, A. H.; Hassan, H.; Ahmad, M. A.; et al. Co-pyrolysis of biomass and waste plastics for production of chemicals and liquid fuels: A review on the role of plastics and catalyst types. *Arabian J. Chem.* **2023**, *16* (1), No. 104389.

(19) Tekade, S. P.; Gugale, P. P.; Gohil, M. L.; et al. Pyrolysis of waste polyethylene under vacuum using zinc oxide. *Energy Sources, Part A* **2025**, *47* (1), 3597−3610.

(20) Kalauni, K.; Vedrtnam, A.; Sharma, S. P.; et al. A comprehensive review of recycling and reusing methods for plastic waste focusing Indian scenario. *Waste Manage. Res.* **2025**, *43* (9), 1378−1399.

(21) Aisien, F. A.; Aisien, E. T. Production and Characterization of Liquid Oil from the Pyrolysis of Waste High-Density Polyethylene Plastics Using Spent Fluid Catalytic Cracking Catalyst. *Sustainable Chem. Clim. Action* **2023**, *2*, No. 100020.

(22) Natesakhawat, S.; Weidman, J.; Garcia, S.; et al. Pyrolysis of high-density polyethylene: Degradation behaviors, kinetics, and product characteristics. *J. Energy Inst.* **2024**, *116*, No. 101738.

(23) Coutinho, D. M.; França, D.; Vanini, G.; et al. Understanding the Molecular Composition of Petroleum and Its Distillation Cuts. *Fuel* **2022**, *311*, No. 122594.

(24) Tessarolo, N. S.; Silva, R. C.; Vanini, G.; et al. Assessing the chemical composition of bio-oils using FT-ICR mass spectrometry and comprehensive two-dimensional gas chromatography with time-of-flight mass spectrometry. *Microchem. J.* **2014**, *117*, 68−76.

(25) Tessarolo, N. S.; Silva, R. V.; Vanini, G.; et al. Characterization of thermal and catalytic pyrolysis bio-oils by high-resolution techniques: 1H NMR, GC × GC-TOFMS and FT-ICR MS. *J. Anal. Appl. Pyrolysis* **2016**, *117*, 257−267.

(26) de Sousa, R. C.; Costa, A. B. S.; Freitas, M. D. M.; et al. Convective drying of black pepper: Experimental measurements and mathematical modeling of the process. *Food Bioprod. Process.* **2024**, *143*, 102−116.

(27) Peçanha, R. P. Particulate Systems. In *Unit Operations Involving Particles and Fluids*; Elsevier: Campus, Rio de Janeiro, 2014.

(28) Massarani, G. *Fluidodinâmica em Sistemas Particulados*; E-papers, 2002. Chapter 2.

(29) Lu, J. J.; Chen, N. W. H. Investigation on the ignition and burnout temperatures of bamboo and sugarcane bagasse by thermogravimetric analysis. *Appl. Energy* **2015**, *160*, 49−57.

(30) de Carvalho, R. F.; de Holanda Pasolini, V.; Breciani, J. G. F.; et al. Poultry manure combustion parameters to produce bioenergy: A thermogravimetric analysis by isoconventional models and machine learning. *Case Stud. Therm. Eng.* **2024**, *53*, No. 103757.
(31) Jia, G. Combustion Characteristics and Kinetic Analysis of Biomass Pellet Fuel Using Thermogravimetric Analysis. *Processes* **2021**, *9*, No. 868.
(32) Friedman, H. L. Kinetics of thermal degradation of char-forming plastics from thermogravimetry. Application to a phenolic plastic. *J. Polym. Sci., Part C: Polym. Symp.* **1964**, *6* (1), 183−195.
(33) Alam, M.; Bhavanam, A.; Jana, A.; et al. Co-pyrolysis of bamboo sawdust and plastic: Synergistic effects and kinetics. *Renewable Energy* **2020**, *149*, 1133−1145.
(34) Özsin, G.; Kılıç, M.; Apaydin-Varol, E.; et al. A thermo-kinetic study on co-pyrolysis of oil shale and polyethylene terephthalate using TGA/FT-IR. *Korean J. Chem. Eng.* **2020**, *37* (11), 1888−1898.
(35) Sbirrazzuoli, N. Advanced isoconversional kinetic analysis: Insight in mechanisms and simulations. Successes and future. *Thermochim. Acta* **2024**, *733*, No. 179688, DOI: 10.1016/j.tca.2024.179688.
(36) Khedri, S. Kinetic and Thermodynamic Studies on Pyrolysis of Waste HDPE Polymers 2017 http://knowledgecommons.lakeheadu.ca/handle/2453/4247.
(37) Ahmad, I.; Khan, M. I.; Khan, H.; et al. Pyrolysis study of polypropylene and polyethylene into premium oil products. *Int. J. Green Energy* **2015**, *12* (7), 663−671.
(38) Alves, J. L. F.; da Silva, J. C. G.; da Silva Filho, V. F.; et al. Kinetics and thermodynamics parameters evaluation of pyrolysis of invasive aquatic macrophytes to determine their bioenergy potentials. *Biomass Bioenergy* **2019**, *121*, 28−40.
(39) Kaur, R.; Gera, P.; Jha, M. K.; et al. Pyrolysis kinetics and thermodynamic parameters of castor (Ricinus communis) residue using thermogravimetric analysis. *Bioresour. Technol.* **2018**, *250*, 422−428.
(40) Tose, L. V.; Cardoso, F. M.; Fleming, F. P.; et al. Analyzes of Hydrocarbons by Atmosphere Pressure Chemical Ionization FT-ICR Mass Spectrometry Using Isooctane as Ionizing Reagent. *Fuel* **2015**, *153*, 346−354.
(41) Souza, L. M.; Tose, L. V.; Cardoso, F. M. R.; et al. Evaluating the Effect of Ion Source Gas (N2, He, and Synthetic Air) on the Ionization of Hydrocarbon, Condensed Aromatic Standards, and Paraffin Fractions by APCI(+)FT-ICR MS. *Fuel* **2018**, *225*, 632−645.
(42) Madhu, G.; Bhunia, H.; Bajpai, P. K.; et al. Mechanical and morphological properties of high density polyethylene and polylactide blends. *J. Polym. Eng.* **2014**, *34* (9), 813−821.
(43) Das, P.; Tiwari, P. Thermal degradation study of waste polyethylene terephthalate (PET) under inert and oxidative environments. *Thermochim. Acta* **2019**, *679*, No. 178340.
(44) Furukawa, T.; Sato, H.; Kita, Y.; et al. Molecular Structure, Crystallinity and Morphology of Polyethylene/Polypropylene Blends Studied by Raman Mapping, Scanning Electron Microscopy, Wide Angle X-Ray Diffraction, and Differential Scanning Calorimetry. *Polym. J.* **2006**, *38*, 1127−1136.
(45) Sinfrônio, F. S. M.; Santos, J. C. O.; Pereira, L. G.; et al. Kinetic of thermal degradation of low-density and high-density polyethylene by non-isothermal thermogravimetry. *J. Therm. Anal. Calorim.* **2005**, *79* (2), 393−399.
(46) Chee, A. L. K.; Chin, B. L. F.; Goh, S. M. X.; et al. Thermo-catalytic co-pyrolysis of palm kernel shell and plastic waste mixtures using bifunctional HZSM-5/limestone catalyst: Kinetic and thermodynamic insights. *J. Energy Inst.* **2023**, *107*, No. 101194.
(47) Meena, P.; Bhoi, R. Thermodynamic and kinetic analysis of waste plastic pyrolysis: Synergistic effects and sustainability perspectives. *Next Sustainability* **2025**, *5*, No. 100132.
(48) Kumbar, P. R.; Patil, V. S.; Kumbar, S. R.; et al. Production and characterization of wax and grease from waste plastic. *IOP Conf. Ser.:Mater. Sci. Eng.* **2021**, *1126* (1), No. 012037, DOI: 10.1088/1757-899x/1126/1/012037.
(49) Marchetti, L.; Guastaferro, M.; Vaccari, M.; et al. Feasibility Study of Renewable Recycled Carbon Fuel Production via Plastic Waste Pyrolysis. *J. Cleaner Prod.* **2025**, *495*, No. 145035.
(50) Laghezza, M.; Fiore, S.; Berruti, F. A Review on the Pyrolytic Conversion of Plastic Waste into Fuels and Chemicals. *J. Anal. Appl. Pyrolysis* **2024**, *179*, No. 106479.
(51) Snow, J.; Kuráň, P.; Kašpárek, A.; et al. Virgin Polymers via Pyrolysis − A Review of Heteroatom Removal Options. *Fuel Process. Technol.* **2024**, *254*, No. 108031.
(52) Belbessai, S.; Azara, A.; Abatzoglou, N. Recent Advances in the Decontamination and Upgrading of Waste Plastic Pyrolysis Products: An Overview. *Processes* **2022**, *10* (4), No. 733.
(53) Schymanski, E. L.; Singer, H. P.; Slobodnik, J.; et al. Non-Target Screening with High-Resolution Mass Spectrometry: Critical Review Using a Collaborative Trial on Water Analysis. *Anal Bioanal Chem.* **2015**, *407* (21), 6237−6255.
(54) Marshall, A. G.; Rodgers, R. P. Petroleomics: The Next Grand Challenge for Chemical Analysis. *Acc. Chem. Res.* **2004**, *37* (1), 53−59.
(55) Pedersen, H.; Conti, T. F. Improving the Circular Economy via Hydrothermal Processing of High-Density Waste Plastics. *Waste Manage.* **2017**, *68*, 24−31.
(56) Kumar, S.; Singh, R. K. Recovery of Hydrocarbon Liquid from Waste High Density Polyethylene by Thermal Pyrolysis. *Braz. J. Chem. Eng.* **2011**, *28* (4), 659−667.

https://doi.org/10.1021/acs.energyfuels.5c06298
Energy Fuels XXXX, XXX, XXX−XXX